Atmos. Chem. Phys., 25, 11975–11989, 2025
https://doi.org/10.5194/acp-25-11975-2025

Atmospheric Chemistry and Physics
Open Access
EGU

Research article

Effects of anthropogenic pollutants on biogenic secondary organic aerosol formation in the atmosphere of Mt. Hua, China

Can Wu[1,2], Yubao Chen[1], Yuwei Sun[1], Huijun Zhang[1], Si Zhang[1], Cong Cao[3,a], Jianjun Li[3], and Gehui Wang[1,2]

[1]Key Lab of Geographic Information Science of the Ministry of Education, School of Geographic Sciences, East China Normal University, Shanghai 210062, China
[2]Institute of Eco-Chongming, 3663 North Zhongshan Road, Shanghai 200062, China
[3]State Key Laboratory of Loess and Quaternary Geology, Institute of Earth Environment, Chinese Academy of Sciences, Xi'an 710061, China
[a]now at: Department of Chemistry, Hong Kong University of Science and Technology, Hong Kong, China

Correspondence: Gehui Wang (ghwang@geo.ecnu.edu.cn)

Received: 8 April 2025 – Discussion started: 15 April 2025
Revised: 23 June 2025 – Accepted: 27 July 2025 – Published: 2 October 2025

Abstract. Anthropogenic effects on biogenic secondary organic aerosol (BSOA) formation in the upper boundary layer are still not fully understood. Here, a synchronized 4-hourly monitoring of three typical BSOA tracers from isoprene, monoterpenes, β-caryophyllene, and other particulate pollutants was conducted at the mountain foot (MF, 400 m above sea level (m a.s.l.)) and mountainside (MS, 1120 m a.s.l.) of Mt. Hua, China, to investigate the chemical evolution of BSOA in air mass lifting. Our findings revealed that BSOA was the predominant source of organic matter (OM) at the MS site, with an average fraction of $\sim 43\,\%$ being ~ 7-fold that at the MF site. As the prevalent BSOA tracer, the isoprene-derived SOA tracers ($BSOA_I$) stayed at a comparable level at the MF site ($183 \pm 81\,ng\,m^{-3}$) and MS site ($197 \pm 127\,ng\,m^{-3}$) yet exhibited an inverse diurnal pattern between the two sites. And the $BSOA_I$ fraction in OM aloft moderately decreased during the daytime and correlated positively with the 2-methyltetrol/2-methylglyceric acid ratio but negatively with NO_x transported from ground level, indicating that anthropogenic NO_x significantly affected the daytime BSOA formation aloft by inhibiting the HO_2•-pathway products. Additionally, the further formation of sulfate in a lifting air mass significantly enhanced aerosol water content aloft, which suppressed the reactive uptake of isoprene epoxydiol and ultimately diminished the $BSOA_I$ yields during the daytime. These findings provide more insight into the intricate anthropogenic–biogenic interactions affecting BSOA formation in the upper boundary layer.

1 Introduction

Volatile organic compounds (VOCs) play a crucial role in atmospheric chemistry (Mcfiggans et al., 2019; Coggon et al., 2021), exerting profound influences on the atmospheric oxidizing capacity, tropospheric ozone burden, and regional climate (Mellouki et al., 2015; Wu et al., 2020). Among the diverse VOCs, biogenic VOCs (BVOCs) primarily emitted by terrestrial vegetation predominate the global VOC flux at $1\,Pg\,yr^{-1}$ (Guenther et al., 2012), exceeding anthropogenic sources by an order of magnitude. The high reactivity of dominant BVOCs (particularly, isoprene, monoterpene, and sesquiterpenes) towards O_3, OH• and NO_3• can drive rapid formation of secondary organic aerosol (SOA) (Zhang et al., 2018a; Ng et al., 2017). Consequently, this biogenically derived SOA (BSOA) would represent a prominent contribution to the global SOA budget (Kelly et al., 2018; Hodzic et al., 2016), although models remain highly uncertain in BSOA prediction owning to the complexity of physicochemical processes involved (Hallquist et al., 2009). Given the sig-

nificant climate interactions and public health implications of BSOA (Scott et al., 2014; Shrivastava et al., 2017), advancing the understanding of BSOA, including its precursors and formation processes, is urgently needed.

Over the past two decades, mounting evidence indicates that anthropogenic pollutants (e.g., SO_2, NO_x) critically regulate the BSOA formation through altering oxidation pathways and gas-to-particle partitioning processes (Xu et al., 2015, 2016; Zheng et al., 2023). For example, sulfate, acting as an effective nucleophile, greatly promotes ring-opening reactions of isoprene epoxydiols (IEPOX) and subsequent SOA formation, particularly organosulfates and corresponding oligomers (Cooke et al., 2024a; Xu et al., 2015). These products contribute significantly to IEPOX-driven SOA and can alter aerosol physicochemical properties (e.g., phase state, viscosity, and morphology) (Lei et al., 2022; Riva et al., 2019), thereby kinetically mediating the reactive uptake of IEPOX, as well as the following SOA yield and evolution (Drozd et al., 2013; Zhang et al., 2018b; Armstrong et al., 2022). Furthermore, a recent laboratory study demonstrates that sulfate/bisulfate equilibrium also plays a critical role in BSOA formation, especially under highly acidic conditions (Cooke et al., 2024b). NO_x as an important driver for BSOA formation could alter the fate of organo-peroxy radicals ($RO_2\bullet$) and subsequently affect the yield and chemical composition of BVOC-oxidized products by changing oxidation pathways (Lin et al., 2013; Pye et al., 2010). Specifically, $RO_2\bullet + HO_2\bullet$ reactions under low NO_x conditions would predominantly yield low-volatility hydroperoxide species; Conversely, the reaction of NO with $RO_2\bullet$ in the high-NO_x regime will produce organonitrates and alkoxy radicals ($RO\bullet$) that can fragment into more volatile products, whereas the impact of NO_x on BSOA yield is nonlinear as explored by laboratory studies (Xu et al., 2014; Kroll et al., 2006). Additionally, the abundant O_3 could also significantly promote BSOA formation by enhancing BVOC ozonolysis. Therefore, the changes of anthropogenic emissions would potentially perturb the BSOA formation. As modeling studies demonstrated, anthropogenic emission controls substantially decreased the BSOA formation in the United States during 1990–2012 (Ridley et al., 2018), and a further $\sim 35\,\%$ of isoprene-derived SOA (SOA_I) would be reduced in 2025 under similar emission regulations (Marais et al., 2016). Parallel effects also emerged in China, where the effective control on SO_2 emissions drove a significant decline of SOA_I at $-8.0\,\%\,yr^{-1}$ over 2007–2015, being 2-fold that of SO_4^{2-} (Dong et al., 2022).

Numerous studies have comprehensively characterized the surface BSOA, yet the vertical distribution of BSOA remains insufficiently understood, which is a critical driver of uncertainties in global climate models (Nazarenko et al., 2017; Hodnebrog et al., 2014). The mountain-based observations revealed that BSOA constitutes a substantial fraction (30 %–60 %) of aerosols in the free troposphere (Fu et al., 2014; Ren et al., 2019; Yi et al., 2021), and this elevated BSOA is significantly influenced by the valley breeze that could transport the surface pollutants to the upper boundary layer, indicating the potential effects of surface pollutant emissions on BSOA formation aloft. In addition, airborne pollutants likely undergo aging in the vertical transport process (Wu et al., 2022), causing increasingly complex compositions and changes in oxidizing capacity and aerosol properties compared with that at ground level. Consequently, more observational studies are necessary to obtain an improved understanding of the anthropogenic–biogenic interactions driving BSOA formation aloft.

Guanzhong Basin of inland China is a typical semiarid region in East Asia, suffering serious particle pollution due to the large anthropogenic emissions (Wang et al., 2016). In our previous studies (Li et al., 2013; Wang et al., 2012), the molecular distribution, evolutionary mechanism, and sources of BSOA have been investigated, whereas the anthropogenic emissions experienced dramatic changes recently in this region (Zhang et al., 2019a); therefore, the primary factors currently driving the BSOA formation are probably distinct from those that prevailed previously. To elucidate the formation mechanism of biogenic SOA aloft in this region, synchronous observations were conducted on the mountainside and the mountain foot of Mt. Hua, which adjoins the Guanzhong Basin. In this study, we firstly investigate chemical molecular compositions and diurnal variation of BSOA over Mt. Hua, then explore the impacts of anthropogenic pollutants on BSOA formation during the vertical transport, and finally quantify its source contributions.

2 Experiment

2.1 Sample collection

From 27 August–17 September 2016, aerosol sampling with a 4 h interval was synchronously conducted at two locations in the Mt. Hua region, employing high-volume air samplers with a flow rate of $1.13\,m^3\,min^{-1}$. One sampling site (34°32′ N, 110°5′ E, 400 m a.s.l; MF) is situated at the mountain foot of Mt. Hua, enveloped by several traffic arteries, residential and commercial buildings. Another site is located on the mountainside (34°29′ N, 110°3′ E, 1120 m a.s.l; MS), approximately 8 km away from the MF site in horizontal distance. This site is adjacent to one of the larger valleys of Mt. Hua, characterized by precipitous terrain and less anthropogenic activity. The surface-level pollutants can be transported to here by the prevailing valley breeze, which has been validated by the organic tracers and meteorological fields simulated by the WRF-Chem model in our previous studies (Wu et al., 2022, 2024). All the aerosol samples were collected on pre-combusted (450 °C for 6 h) quartz filters (Whatman 1851–865), which have a retention efficiency of $> 99.995\,\%$ for dioctyl phthalate particles at 0.3 µm. After collection, the filter samples were stored in a freezer ($< -18\,°C$) prior to chemical analysis.

Additionally, the hourly concentrations of the pollutants, including $PM_{2.5}$, O_3, and NO_2, were also monitored at the MS site by corresponding online equipment, while data for the MF site were mainly acquired through Weinan Ecological Environment Bureau (http://sthjj.weinan.gov.cn/, last access: 8 July 2021). All meteorological data were downloaded from the Shaanxi Meteorological Bureau website (http://sn.cma.gov.cn/, last access: 8 July 2021). The comprehensive details regarding the sampling sites and instrumentation were delineated in our previous studies (Wu et al., 2022, 2024).

2.2 Chemical analysis

The details of organic matter extraction, derivatization, and gas chromatography/mass spectrometry (GC/MS) analyses can be found elsewhere (Wang and Kawamura, 2005). Briefly, for the analytical procedure of organic tracers in the aerosol, one-quarter of $PM_{2.5}$ sample was cut into pieces and then ultrasonically extracted with a mixture of dichloromethane and methanol (2 : 1, v/v) three times (each for 15 min). The extracts were filtered through a pasteur pipette plugged with quartz wool into a pear-shaped bottle. The filtrates were concentrated by a rotary evaporator under vacuum state and then dried by pure nitrogen. After reaction with 60 µL derivatization reagent (a mixture of 50 µL of N,O-*bis*-(trimethylsilyl)trifluoroacetamide (BSTFA) and 1 % trimethylsilyl chloride and 10 µL of pyridine) for 3 h at 70 °C in order to convert COOH and OH groups to the corresponding trimethylsilyl esters and ethers and cooling down to room temperature, an aliquot of 40 µL internal standard (C_{13} *n*-alkene) was added into the derivative solution prior to GC/MS analyses. All BSOA tracers were individually identified by comparing mass spectra against authentic standards and literature data, whereas, due to the commercial unavailability of a subset of authentic standards, the quantification of target compounds relied on the surrogate standards, expect for *cis*-pinonic. Specifically, erythritol was applied to determine the 2-methyltetrols, C_5-alkene triols, and 3-MeTHF-3,4-diols. The quantification of 2-methylglyceric acid, 3-hydroxyglutaric acid, 3-methyl-1,2,3-butanetricarboxylic acid, and β-caryophyllinic acid was performed using glyceric acid, tartaric acid, suberic acid and *cis*-pinic acid, respectively. This approach was also applied in other similar studies (Li et al., 2013; Zhu et al., 2016). The standard solutions were spiked onto the blank filters to assess to the recoveries, which ranged from 82 %–105 %. Field blank filters were also analyzed following the same analytical procedure as the ambient samples, with no target compounds detected in these blanks.

Furthermore, partial filters were cut into pieces and then extracted three times under sonication with 15 mL Milli-Q pure water (18.2 MΩ). A total of 10 ions such as SO_4^{2-}, NO_3^-, Cl^-, NH_4^+, and K^+ were determined using ion chromatography (Dionex, ICS-1100). A DRI model 2001 thermal–optical carbon analyzer was used to measure the organic carbon (OC) and element carbon (EC) in each $PM_{2.5}$ filter sample, from which water-soluble organic carbon (WSOC) was extracted into Mill-Q pure water (18.2 MΩ) and ultimately quantified by a total organic carbon (TOC) analyzer (Model TOC-L CPH, Shimadzu, Japan).

2.3 Aerosol liquid water content (ALWC) and in situ pH

The thermodynamic model (ISORROPIA-II) can provide robust predictions of the aerosol liquid water content (ALWC) and in situ pH in $PM_{2.5}$ samples. By combining the actual temperature (T) and relative humidity (RH) in the atmosphere and the composition, the ALWC and H^+ loads can be simulated, which are used for calculating the in situ pH.

2.4 Positive matrix factorization (PMF) source apportionment

As a receptor model, PMF is a mathematical approach to quantify the contribution of sources to samples and has been widely used in the source apportionment of air pollutants. More details on the model can be found on the EPA website (http://www.epa.gov/air-research/epa-positive-matrix-factorization-50-fundamentals-and-user-guide, last access: 16 May 2024). In this work, the organic matter (OM), EC WSOC, secondary inorganic ions, and biogenic SOA of all the samples served as the fingerprint species to identify potential sources of the BSOA at Mt. Hua. After extensive testing, the model output an optimal solution characterized by a minimal difference between Q_{True} and Q_{Robust} and a Q/Q_{expected} ratio approaching 1. This is indicative of the robust model performance, as confirmed by the high correlation coefficients between input and estimated values. Furthermore, as revealed in our pervious study (Wu et al., 2022), the change of the main emission sources was insignificant in the air mass lifting process on Mt. Hua. Thus, the samples from both sites were added together as one data matrix. Based on the Q values (Q_{True}: 2362.8 vs. Q_{Robust}: 2365.6; Q/Q_{expected}: 0.86) and interpretability, five factors were obtained as the optimal solution after numerous testes. And the model could commendably reconstruct the temporal profiles of the input species, showing significant correlations ($R^2 > 0.92$) between observed and simulated species.

2.5 Concentration-weighted trajectory (CWT) analysis

To identify the potential spatial sources of the high BSOA on Mt. Hua, a CWT analysis was conducted using the BSOA concentrations and air mass backward trajectories. The 12 h backward trajectories at a height of 1100 m were calculated by the Hybrid Single-Particle Lagrangian Integrated Trajectory (HYSPLIT) model on an hourly basis throughout the campaign. Due to the relatively low temporal resolution of filter samples, the averaged BSOA concentration was as-

signed to match all the trajectories corresponding to each sample. And the CWT analysis herein was subsequently performed using an Igor-based tool (i.e., ZeFir v3.70); more details for the protocol can be found in Petit et al. (2017). Briefly, a grid with $0.25° \times 0.25°$ cell size was created to cover all the trajectories. Each grid cell was assigned a weighted concentration, which was obtained from the averaged BSOA concentration with associated trajectories crossing the grid cell. A high value in a grid cell indicates that the air parcels passing through it were associated with a high concentration at the receptor site.

3 Results and discussion

3.1 Overview of OM during the campaign

The bulk chemical compositions of $PM_{2.5}$ during the campaign have been reported in our previous work (Wu et al., 2022) and strongly substantiated the fact that organic matter (OM) is the principal component of $PM_{2.5}$ at both surface and high-elevation sites, with a mass fraction of 32 %–46 %. For a deeper insight into the relative abundances, vertical variability, and sources of OM between the two sampling sites, a comprehensive comparison is presented in Fig. 1. The OM concentration was $30 \pm 10\,\mu g\,m^{-3}$ at the surface, approximately 3-fold that aloft. Such abundant OM at the surface was apparently driven by fresh emissions from nearby roads and residences, as evidenced by its strong correlation with hopanes (Fig. S1a in the Supplement, $R^2 = 0.46$, $p < 0.05$), being a known tracer for combustion sources (Schauer et al., 1999), whereas a weak correlation between OM and hopanes was found at the MF site, indicating different sources for the OM aloft. Moreover, the surface OM was characterized by a higher nocturnal load and exhibited a decreased trend before midafternoon (Fig. S1b), which was thermally driven boundary layer growth. Nonetheless, an inverse diel pattern was observed at a high-elevation site with a daily OM peak at the moment (12:00–16:00 GMT+8) of strong photochemical activity (Fig. S1b), suggesting that OM components aloft were probably driven by photochemistry.

To determine the sources of OM at both sites, we performed a positive matrix factorization (PMF) analysis and identified five types of sources for OM (Fig. S2). Among these sources, biomass burning (BB) and fossil fuel combustion were believed to be the primary sources for OM at the surface, accounting for 52 % and ∼ 18 % of OM (Fig. 1c), respectively. This coincided with values in Xi'an (∼ 43 % for BB) and Lin Village (30 %–40 % for BB) located on the Guanzhong plain (Elser et al., 2016; Li et al., 2022), whereas merely ∼ 24 % of OM was explained by the above anthropogenic sources at the MS site, and most of the OM aloft was dominated by biogenic secondary organic aerosol (BSOA, Fig. 1d), with a fractional contribution of ∼ 43 % being 7-fold that for subaerial OM. This indicates a significant influence of biogenic primary and secondary sources on OM aloft.

3.2 Abundance and spatiotemporal variations of BSOA tracers

To characterize the spatiotemporal variations of biogenic SOA between the two sites, plenty of BSOA tracers including isoprene, monoterpene, and sesquiterpene were quantified as summarized in Table 1. The sum of detected BSOA tracers ranged 31–459 $ng\,m^{-3}$ at the MF site ($269 \pm 108\,ng\,m^{-3}$, Fig. S3), which was slightly lower than that at the MS site ($277 \pm 159\,ng\,m^{-3}$). Such a spatial pattern was also observed at Mt. Tai on the North China Plain (Yi et al., 2021), further underscoring the significance of biogenic sources in mountainous OM formation aloft. Specifically, isoprene SOA tracers ($BSOA_I$) as the dominant species accounted for ∼ 70 % of the identified BSOA tracers, with an average of $197 \pm 127\,ng\,m^{-3}$ at the MS site and $183 \pm 81\,ng\,m^{-3}$ at the MF site, respectively. These were comparable to that in the Kathmandu Valley of India ($183 \pm 81\,ng\,m^{-3}$) (Wan et al., 2019) and a midlatitudinal forest zone (∼ $240\,ng\,m^{-3}$) (Zhu et al., 2016) but ∼ 2 orders of magnitude higher than those measured over the North Pacific ($3.6\,ng\,m^{-3}$) (Fu et al., 2011). As for total monoterpene SOA tracers ($BSOA_M$) and sesquiterpene tracers ($BSOA_S$), their abundances were lower by a factor of approximately 4–6 than $BSOA_I$, probably due to lower emissions of monoterpene and sesquiterpene from the vegetation in this region. Noteworthily, $BSOA_M$ exhibited a converse spatial pattern, with a high load at the surface (MF: $52 \pm 23\,ng\,m^{-3}$ vs. MS: $32 \pm 20\,ng\,m^{-3}$). The coniferous plants, as primary emitters of monoterpene (Gagan et al., 2023), may be less densely distributed at the ground level relative to that on Mt. Hua. Thus, relatively abundant $BSOA_M$ at the surface is likely affected by intensive BB activities that can also release numerous monoterpenes, thereby potentially augmenting the surface $BSOA_M$ levels. This can be manifested by that $BSOA_M$ strongly correlated with levoglucosan, being known as a BB tracer, but weakly with C_{29}-alkane that mainly derived from vegetation emissions (Wang and Kawamura, 2005) (Fig. S4).

3.2.1 Isoprene SOA tracers

A total of eight isoprene tracers formed by oxidated reactions of isoprene with NO_x and OH_2• were identified in this study, namely C_5-alkene triols (*cis*-2-MTB, *trans*-2-MTB and 3-MTB), 2-MGA, 2-methyltetrols (2-MT and 2-ME), and 3-MeTHF-3,4-diols (*trans*-3-Methyltetrahydrofuran-3,4-diol, and *cis*-3-Methyltetrahydrofuran-3,4-diol). The $BSOA_I$ at the MF site exhibited a pronounced diurnal cycle, characterized by a higher daytime load with an afternoon peak of $210 \pm 96\,ng\,m^{-3}$ (Fig. 2a). This pattern aligns with temperature-driven characteristic of isoprene emission (Pétron et al., 2001; Zeng et al., 2023). A positive correla-

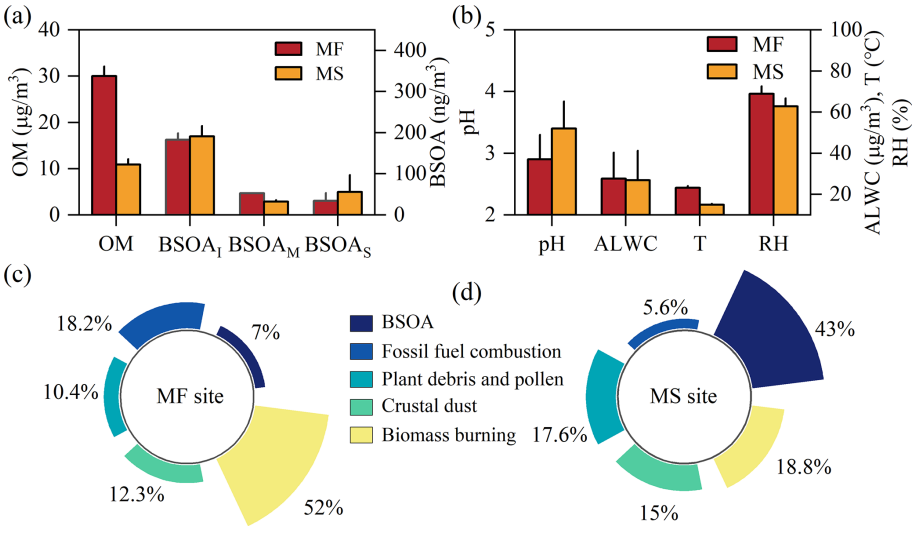

Figure 1. Comparisons of chemical composition **(a)**, meteorological conditions **(b)**, and sources for OM **(c, d)** between the two sampling sites. OM concentration is converted by the OM/OC ratio measured in our previous (Wu et al., 2024). The standard deviations of all species except BSOAs in **(a)** and **(b)** were reduced by a factor of 5.

tion between $BSOA_I$ and temperature ($R^2 = 0.63$) implies that a substantial part of surface $BSOA_I$ was expected to be formed locally (Fig. S5a), given the short atmospheric lifetime of isoprene, whereas $BSOA_I$ aloft was characterized by an inverse diurnal variation, with a moderate enhancement in the nocturnal load. As revealed by a high-elevation CWT analysis of $BSOA_I$ (Fig. 3), relatively high nocturnal loading was distributed over Mt. Hua and adjacent regions, indicating that these SOA tracers aloft were significantly influenced by regional/super-regional transport, especially during the nighttime.

2-Methyltetrols (2-MTLs), as the predominant species at both sites, were more abundant aloft ($99 \pm 69\,ng\,m^{-3}$) relative to the surface site ($74 \pm 32\,ng\,m^{-3}$). The levels were comparable to the field measurements at Mt. Tai ($98\,ng\,m^{-3}$) (Yi et al., 2021), Mt. Changbai ($22–282\,ng\,m^{-3}$) (Wang et al., 2008), and Mexico City ($8–190\,ng\,m^{-3}$) (Cooke et al., 2024a). Recently, a forest observation demonstrated that 2-MTLs could be biologically produced and then directly emitted into the atmosphere (Ye et al., 2021), whereas there is no significant correlation between 2-MTLs and C_{29}-alkane mainly released by vegetation (Fig. S4b), indicating that 2-MTLs at both sampling sites primarily derived from secondary formation rather than being directly emitted by vegetation. As the oxidation products of isoprene under low/free-NO_x conditions, 2-MTLs at the MF site were significantly formed during the daytime and peaked at 12:00–16:00 LT (local time, $85\,ng\,m^{-3}$, Fig. 2b), corresponding to the period of reduced NO_x loads, high temperature, and intense solar radiation. Conversely, the concentration of 2-MTLs aloft decreased progressively during the daytime, bottoming out at 16:00–20:00 LT. This inverse diurnal pattern was probably due to the influx of the surface NO_x that was transported aloft by the prevailing valley breeze, which subsequently inhibited the 2-MTL formation aloft. Meanwhile, such relatively abundant NO_x conditions during the daytime promoted the formation of 2-MGA aloft (culminating at 12:00–16:00 LT), as corroborated by a positive correlation between 2-MGA and NO_2 (Fig. S5c). This finding was consistent with the laboratory measurements of 2-MGA derived from oxidization of isoprene with a high NO_x load (Surratt et al., 2006; Szmigielski et al., 2007). Moreover, the surface 2-MGA also exhibited a similar diurnal pattern with an average of $29 \pm 15\,ng\,m^{-3}$, being 1.8-fold that aloft, despite a weak relationship between 2-MGA and NO_2. This appreciably suggested that, beyond NO_x, other factors also drove the 2-MGA formation at the MF site.

C_5-alkene triols and 3-MeTHF-3,4-diols were another prevalent isoprene tracer, concentrations of which were comparable between the two sites (Table 1). As the photooxidation products under low/free-NO_x levels, the above two tracers exhibited a diurnal cycle parallel to that of 2-MTLs at the two sites and were characterized by higher loads during nighttime. Despite that, the correlation between C_5-alkene triols and 3-MeTHF-3,4-diols ($R^2 > 0.74$) was more robust than that involving 2-MTLs. This was probably owing to the fact that C_5-alkene triols and 3-MeTHF-3,4-diols were mainly formed via acid-catalyzed intermolecular rearrangement reactions of epoxy-diols (Lin et al., 2012; Wang et al., 2005), whereas 2-MTLs are likely to result from nucleophilic addition of water to the ring opening of epoxy-diols (Surratt et al., 2010).

Table 1. Summary of the average BSOA tracers at the two sampling sites during the whole campaign.

Compounds	Mountain foot			Mountainside		
	Average	Daytime	Nighttime	Average	Daytime	Nighttime
Isoprene-derived SOA tracers (ng m^{-3})						
2-MGA[a]	29 ± 15	36 ± 17	22 ± 7	16 ± 8	20 ± 9	13 ± 6
2-methyltetrols						
2-Methylthreitol	24 ± 10	25 ± 10	23 ± 10	32 ± 23	29 ± 21	36 ± 24
2-Methylerythritol	50 ± 2	52 ± 23	48 ± 21	67 ± 46	57 ± 42	76 ± 49
subtotal	74 ± 32	77 ± 33	71 ± 31	99 ± 68	86 ± 62	112 ± 72
C_5-alkene triols						
cis-2-Me-1,3,4-THB[b]	20 ± 13	20 ± 13	20 ± 13	22 ± 18	19 ± 15	24 ± 20
3-Me-2,3,4-THB[c]	23 ± 15	22 ± 14	23 ± 16	23 ± 19	21 ± 17	26 ± 21
trans-2-Me-1,3,4-THB[d]	31 ± 19	30 ± 19	31 ± 19	30 ± 22	26 ± 19	33 ± 25
subtotal	74 ± 46	73 ± 45	74 ± 48	75 ± 59	66 ± 51	83 ± 66
3-MeTHF-3,4-diols						
trans-3-Me-THF-diol[e]	3 ± 1	3 ± 1	3 ± 1	3 ± 2	3 ± 2	3 ± 2
cis-3-Me-THF-diol[f]	4 ± 2	4 ± 2	4 ± 2	4.7 ± 3.7	4 ± 3	5 ± 4
subtotal	7 ± 3	7 ± 3	7 ± 3	8 ± 6	8 ± 5	8 ± 6
Total	182 ± 81	191 ± 83	173 ± 77	197 ± 126	178 ± 114	216 ± 135
α / β-pinene-derived SOA tracers (ng m^{-3})						
cis-pinonic acid	9 ± 4	9 ± 4	9 ± 4	4 ± 2	4 ± 2	4 ± 3
pinic acid	5 ± 2	6 ± 2	5 ± 2	3 ± 2	4 ± 2	3 ± 2
MBTCA[g]	26 ± 14	30 ± 14	23 ± 14	19 ± 13	21 ± 14	18 ± 12
3-HGA[h]	12 ± 6	14 ± 6	11 ± 6	6 ± 4	7 ± 5	4 ± 3
Total	52 ± 23	59 ± 22	46 ± 22	32 ± 20	36 ± 21	28 ± 18
β-caryophyllene-derived SOA tracer (ng m^{-3})						
β-Caryophyllinic acid	35 ± 19	35 ± 17	34 ± 20	56 ± 40	70 ± 46	42 ± 28

[a] 2-MGA: 2-methylglyceric acid; [b] *cis*-2-Me-1,3,4-THB: *cis*-2-Methyl-1,3,4-trihydroxy-1-butene; [c] 3-Me-2,3,4-THB: 3-Methyl-2,3,4-trihydroxy-1-butene; [d] *trans*-2-Me-1,3,4-THB: *trans*-2-Methyl-1,3,4-trihydroxy-1-butene; [e] *trans*-3-Me-TH-diol: *trans*-3-Methyltetrahydrofuran-3,4-diol; [f] *cis*-3-Me-TH-diol: *cis*-3-Methyltetrahydrofuran-3,4-diol; [g] MBTCA: 3-methyl-1,2,3-butanetricarboxylic acid; [h] 3-HGA: 3-Hydorxyglutaric acid

3.2.2 Monoterpene SOA tracers

The detected monoterpene tracers, including pinic acid (PA), *cis*-pinonic acid (PNA), 3-hydroxyglutaric acid (3-HGA), and 3-methyl-1,2,3-butanetricarboxylic acid (MBTCA), are mainly derived from photooxidation of α- and β-pinene initiated by •OH and O_3. Therefore, those four tracers exhibited a similar diurnal pattern, peaking at 12:00–16:00 LT when •OH and O_3 concentrations remained at the highest daily level. Based on the chamber measurements, PA and PNA are the early-generation products of α- and β-pinene (Liu et al., 2022; Jaoui et al., 2005), merely accounting for ∼ 10 % and ∼ 12 %–17 % of the $BSOA_M$, respectively. Strikingly, PNA at the two sampling sites was more abundant by a factor of ∼ 1.5 than PA, consistent with the observations at Mt. Tai, Mt. Huang, and Duke Forest, North Carolina (Wang et al., 2023; Bhat and Fraser, 2007; Yi et al., 2021). The saturation vapor pressure of PNA (∼ 7.2×10^{-5} Pa at 298 K, estimated by the E-AIM model) is lower than that of PA (∼ 2.0×10^{-4} Pa); thus, PNA can be readily nucleated and saturated in the atmosphere. Given that, PNA was expected to have a higher abundance in aerosol than PA.

During the campaign, MBTCA was the most abundant $BSOA_M$ tracer, explaining more than half of the surface $BSOA_M$ tracers at both sites, followed by 3-HGA with fractional contributions of ∼ 20 % to total $BSOA_M$. MBTCA and 3-HGA are regarded as the later-generation products of α- and β-pinene and can be derived from further photodegradation of PNA or PA. Thus, the MBTCA/(PA + PNA) ratio (abbreviated as M/P hereafter) is commonly used to estimate the α- and β-pinene-derived SOA aging, a higher value of which is indicative of more aged α- and β-pinene SOA. As depicted in Fig. S6, the M/P value (2.6 ± 1.3) at the MS site was ∼ 1.4-fold that at the MF site, reflecting the fact that the $BSOA_M$ tracers aloft were more aged compared to that at surface. This finding coincided with the variation of the oxidation state of carbon (OSc) measured by the aerosol mass

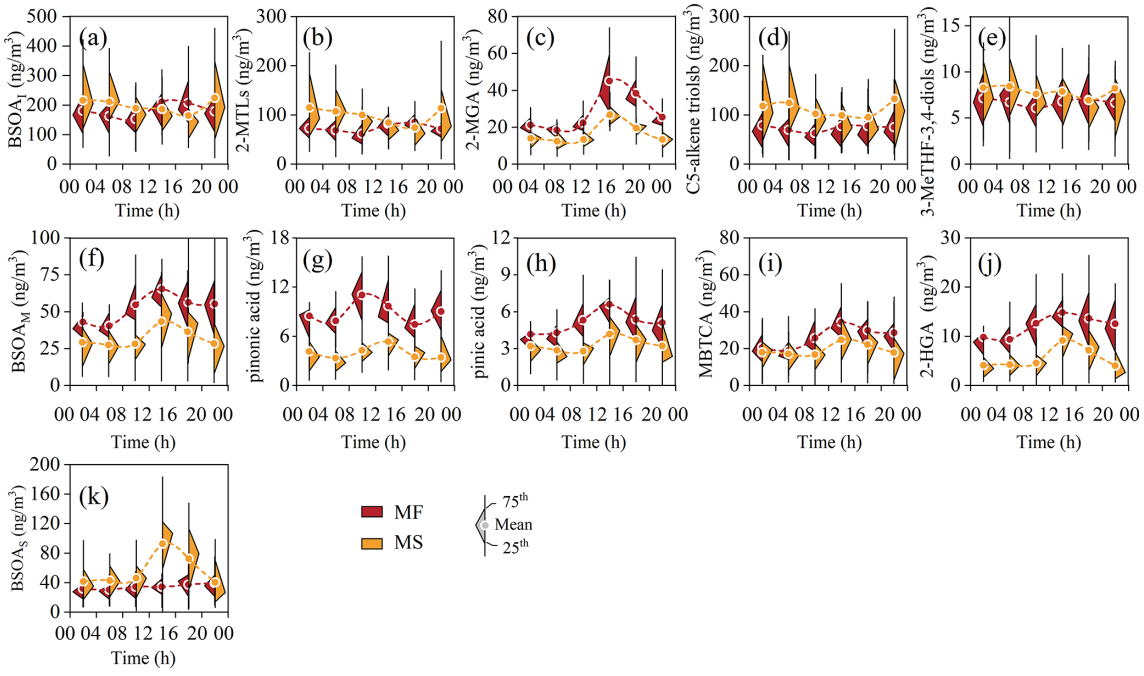

Figure 2. Diurnal variations in BSOA tracers between the two sites. **(a–e)** Isoprene-derived SOA tracer, **(f–j)** monoterpene-derived SOA tracer, and **(k)** β-caryophyllene-derived SOA tracer.

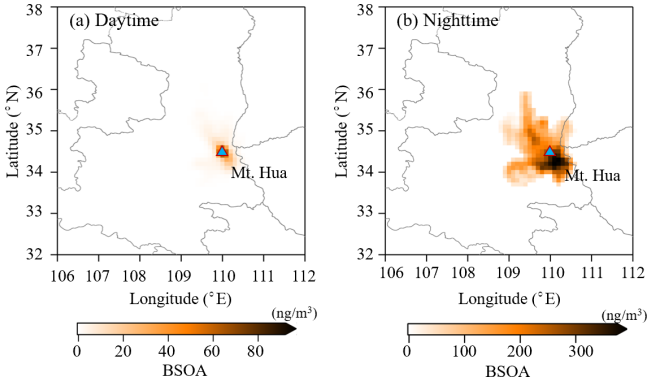

Figure 3. A concentration-weighted trajectory (CWT) analysis for BSOA$_I$ at the MS site.

spectrometer. Additionally, a clear diurnal pattern of M/P ratio was found at the MF site, with a daily peak at 16:00–20:00 LT that lagged that of MBTCA by ∼ 4 h. However, the diurnal cycle of the M/P ratio at the MS site exhibited a bimodal pattern, with two nearly equivalent peaks during the daytime (16:00–20:00) and nighttime (04:00–08:00). Relatively high M/P ratios during nighttime indicated a more aged state of nocturnal α- and β-pinene SOA at the upper atmosphere, markedly differing from the ground-based observations. This was partially due to the fact that the nocturnal pollutants at the MS site were mostly driven by regional or long-range transport (Fig. 3), in which α- and β-pinene SOA aloft would undergo deeper aging, leading to the high M/P ratio.

3.2.3 Sesquiterpene SOA tracers

As a typical and abundant sesquiterpene, β-caryophyllene has been widely studied due to its high reactivity and significant aerosol formation potential; it can be oxidated into β-caryophyllinic acid via ozonolysis/photooxidation (Jaoui et al., 2007, 2003). In this study, β-caryophyllinic acid was found to exhibit a relatively high concentration among the detected BSOA tracers (Table 1), with an average of $35 \pm 19\,\mathrm{ng\,m^{-3}}$ at the MF site and $56 \pm 41\,\mathrm{ng\,m^{-3}}$ at the MS site. These loads were comparable to Mt. Wuyi (7.6–54 ng m^{-3}) (Ren et al., 2019) and Mt. Tai (0.05–48 ng m^{-3}) (Fu et al., 2012). As expected, β-caryophyllinic acid robustly correlated with the BSOA$_M$ ($R^2 > 0.60$, $p < 0.05$) at both sampling sites, indicating similar formation pathways for these species. Additionally, the significant relationship between β-caryophyllinic acid and levoglucosan at the MF site could be a result of intensive biomass burning as indicated in Sect. 3.1. This observation aligns with previous findings that sesquiterpenes accumulated in leaves and wood can be released in the biomass burning process and subsequently oxidized to form β-caryophyllinic acid (Zhang et al., 2019b). Notably, β-caryophyllene SOA tracers aloft in this study showed clearly enhanced concentrations during the daytime from 10:00–16:00 GMT+8, whereas the diurnal cycle of β-caryophyllinic acid at the MF site was less pronounced, de-

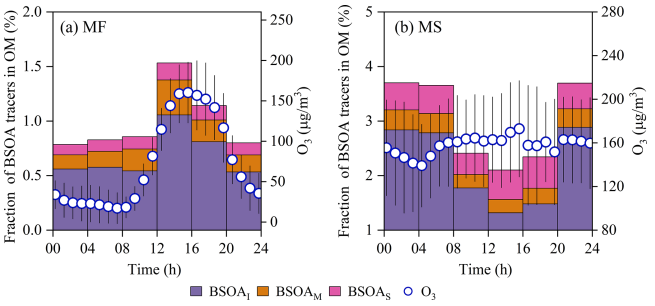

Figure 4. Diurnal cycles of the mass fraction of BSOA tracers in OM and O_3 at both sampling sites.

spite significant diurnal differences in O_3 load and temperature that are known to influence heterogeneous reactions of β-caryophyllene.

3.3 Influencing factors of BSOA formation in the upper troposphere

A comparison of the diurnal cycles of the mass fraction of BSOA to OM ($F_{BSOA/OM}$) between the two sampling sites is illustrated in Fig. 4. At the MF site, a spike in $F_{BSOA/OM}$ was observed at around 12:00–16:00 GMT+8 (Fig. 4a), demonstrating that the surface BSOA formation was strongly enhanced in the presence of abundant O_3/OH radical load and high biogenic emissions, especially for isoprene SOA; such diurnal variation was in good agreement with the measurements at other sites (Zhang et al., 2019b; Zhu et al., 2016; Lee et al., 2016), whereas $F_{BSOA/OM}$ for isoprene aloft exhibited a decreasing pattern during the photochemically active period (Fig. 4b), reaching a minimum at 12:00–16:00 LT. Although oxidant levels remained relatively high at this time, the $F_{BSOA/OM}$ isoprene was only 75 % of that for the prior moment. Our previous observational evidence has corroborated the fact that surface anthropogenic pollutants can be transported to the upper atmosphere by the prevailing valley breeze (Wu et al., 2022, 2024). Those anthropogenic pollutants (e.g., SO_2, NO_x) likely modulated BSOA formation aloft, leading to above unusual diurnal cycle of $F_{BSOA/OM}$ isoprene. To elucidate the above hypothesis, the Mantel test and random forest (RF) analysis were applied for daytime BSOA aloft. More descriptions and settings for the models can be seen in the Supplement (Sect. S1).

3.3.1 Effects of meteorological factors on BSOA

As illustrated in Fig. 5a, the daytime $BSOA_I$ aloft positively correlated with ambient temperature, consistent with the observations on Mt. Tai, Mt. Huang, and Mt. Wuyi (Ren et al., 2019; Wang et al., 2023; Yi et al., 2021). Given the temperature-driven characteristic of isoprene emission (Pétron et al., 2001), relatively high temperature was expected to enhance biogenic SOA yield through the photooxidation of isoprene. while $BSOA_M$ and $BSOA_S$ exhibited insignificantly negative correlations with temperature (Fig. 5a), indicating that their formation may be less sensitive to temperature variations. Additionally, the strong temperature dependence of $BSOA_I$ also indicated that a significant quantity of $BSOA_I$ tracers aloft undergo rapid in situ formation once the oxidant concentrations build up during the daytime, contrasting with those during nighttime. An insignificant correlation was observed between relative humidity and BSOA tracers ($|r| < 0.08$, $P \geq 0.05$). However, moist weather frequently occurred at the MS site, even during the daytime with average RH of 62 ± 19 % (Wu et al., 2022); thus, the less pronounced variation can explain the insensitivity of BSOA formation to RH. Even so, the high RH during the daytime could indirectly influence BSOA formation aloft by modulating aerosol water content (ALWC), aerosol acidity, and gas–particle partitioning of BSOA precursors (Xu et al., 2015; Yan et al., 2025; Isaacman-Vanwertz et al., 2016).

3.3.2 Effects of anthropogenic pollutants on BSOA

Evidence from laboratory studies referred to a nonlinear dependence of BSOA yield on NO_x load, wherein the yield increases with rising NO_x levels under low NO_x conditions but exhibits a decreasing trend as NO_x levels rise under high NO_x conditions (Xu et al., 2014, 2025), whereas the BSOA tracers aloft, especially isoprene-derived SOA, negatively correlated with NO_2 ($r = 0.36$, $P < 0.05$) (Fig. 5a). Additionally, the 2-MTL / 2-MGA ratio, which is indicative of NO_x influence on SOA formation, followed a similar diurnal pattern to that of the $F_{BSOA/OM}$ isoprene (Fig. 5b). All those findings indicated that the NO_2 transported from the surface to high altitude may limit the formation of SOA_I in the daytime. As is well-known, isoprene oxidization primarily follows two pathways, i.e., HO_2 pathway forming 2-MTLs in NO_x-limited conditions and NO/NO_2 channel yielding 2-MGA in high-NO_x scenarios (Surratt et al., 2010; Szmigielski et al., 2007). Thereby, we hypothesized that the increasing NO_x at the MS site may perturb BSOA formation by competing with the HO_2 pathway, diminishing the net SOA yield relative to NO_x-limited conditions. This was consistent with experimental findings by Thornton et al. (2020), who demonstrated that at a high NO_x level (NO $\sim$ 500 ppt) that is akin to our daytime observations at the MS site, the maximum BSOA yield is 10 % lower than that at low NO_x.

As shown in Fig. 5a, sulfate presented a statistically significant positive relationship with $BSOA_I$. This feature appeared to be common for other similar field studies (Wang et al., 2008; Xu et al., 2015; Liu et al., 2017), underscoring the significant role of sulfate in the isoprene-derived SOA formation. According to laboratory studies (Eddingsaas et al., 2010), sulfate can act as nucleophiles to facilitate the ring-opening reaction of IEPOX, which is a pivotal oxidation product of isoprene when organic peroxy radicals mainly react with HO_2 radicals, while the daytime sulfate level was

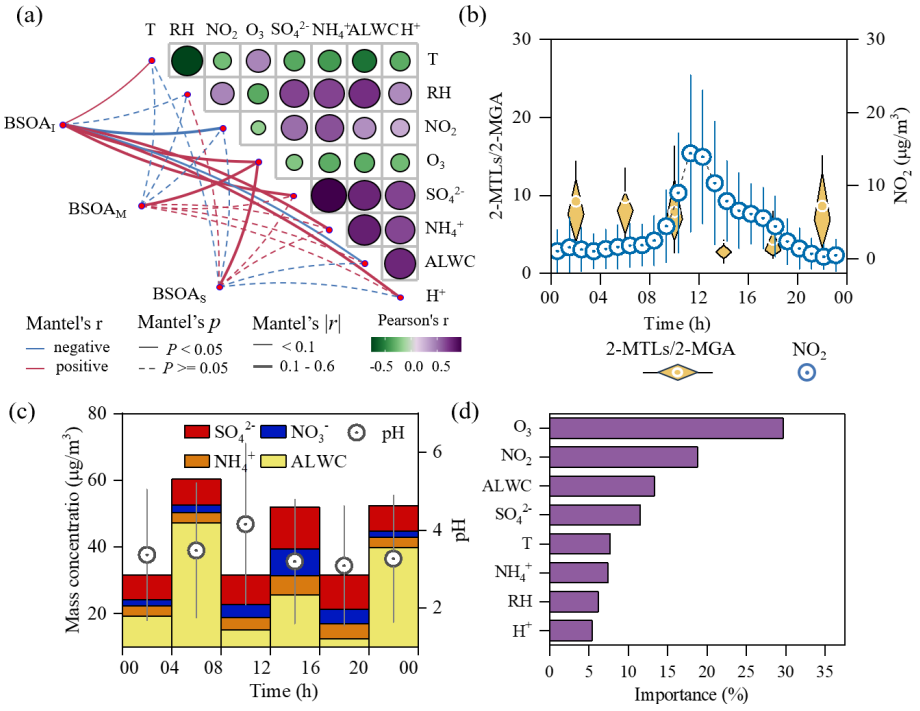

Figure 5. Formation of daytime isoprene-derived SOA in the upper troposphere. **(a)** Mantel test between BSOA tracers and potential influencing factors at the MS site. **(b, c)** Diurnal variations of the 2-MTL / 2-MGA ratio, pH, and the concentration of NO_2, SNA, and ALWC at the MS site. **(d)** Importance assessment for the key factors affecting the daytime isoprene-derived SOA at the MS site.

moderately enhanced, peaking at 12:00–16:00 LT (Fig. 5c). Additionally, a ∼ 4 % enhancement in the mass fraction of daytime sulfate was also observed at the MS site compared to the MF site (Fig. S7a). These findings are indicative of further formation in the air mass lifting process (Wu et al., 2022). An increase in sulfate would boost the ionic strength and salting-in effect of aerosol, thereby enhancing IEPOX reactive uptake and inhibiting its reversible partitioning back to the gas phase. The SO_4^{2-}/HSO_4^- equilibrium is crucial for $BSOA_I$ yield under a highly acidic condition (Cooke et al., 2024b), while the chemical form of inorganic S(VI) also shifts from HSO_4^- at the MF site to SO_4^{2-} at the MS site during vertical transport, which would facilitate $BSOA_I$ formation, as the nucleophilicity of SO_4^{2-} is 2 orders of magnitude higher than that of HSO_4^- (Aoki et al., 2020). As is well-known, sulfate can modulate the H^+ level, acting as a more efficient proton donor to catalyze IEPOX ring opening and isoprene ozonolysis. Thus, the H^+ concentration predicted by the thermodynamic model ISORROPIA II positively correlates with $BSOA_I$ ($r = 0.37$, $P < 0.05$, Fig. 5a). But a nonlinear relationship between the yields of methyltetrol sulfates and 2-MTLs under low pH (< 3) conditions is revealed in the chamber study (Cooke et al., 2024b). Based on our previous study (Wu et al., 2022), the average daytime pH was 3.4±2.2 at the MS site, indicating that there are other factors perturbing BSOA formation at Mt. Hua, warranting further investigation.

Furthermore, the additional sulfate formation in a lifting air mass can also promote an enhancement in ALWC aloft, consistent with the strong positive correlation observed between ALWC and sulfate ($R^2 = 0.66$, $P < 0.05$, Fig. S7). As demonstrated in Fig. 5c, the daytime ALWC peaked at 12:00–16:00 LT, corresponding to a significant decrease in $F_{\text{BSOA isoprene/OM}}$. This pattern suggested an inhibited effect of aerosol water on BSOA formation, consistent with laboratory observation by Gaston et al. (2014), who found a 50 % reduction in IEPOX reactive uptake on NH_4HSO_4 particles as RH increases from 30 %–70 %. As evidenced by previous studies (Xu et al., 2015; Riedel et al., 2015), abundant aerosol water can moderate BSOA formation by affecting ionic strength and proton donor/nucleophilic activity, consequently altering the reactive uptake (e.g., IEPOX) and subsequent reactions. To quantitatively evaluate the effects of ALWC, the pseudo-first-order heterogeneous reaction rate constant for IEPOX reactive uptake (k_{het}) was calculated for the samples at the MS site following the method of Gaston et al. (2014) (Sect. S2). The simulated uptake coefficient of IEPOX (γ_{IEPOX}) during the daytime was 4.3×10^{-4}, being in the range of field and laboratory observations ($0.1 - 6.5 \times 10^{-4}$) (Zhang et al., 2017; Gaston et al., 2014). As shown in Fig. 6, high ALWC commonly corresponds to low γ_{IEPOX} during the daytime, characterized by weak ionic strength and low $H^+_{(aq)}$ concentration. This indicates that enhanced ALWC at MS likely impeded the IEPOX uptake onto a particle sur-

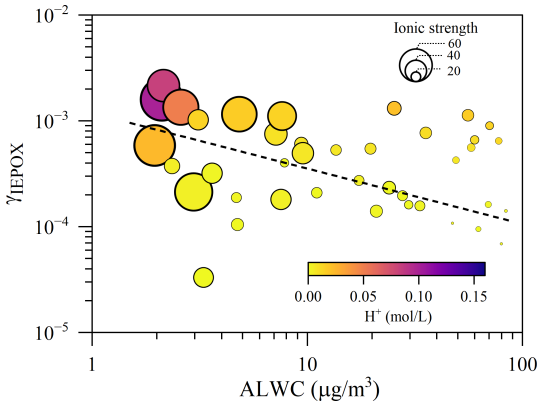

Figure 6. Reactive uptake (γ_{IEPOX}) as a function of ALWC during the daytime at the MS site.

face. Consequently, the average k_{het} at 12:00–16:00 LT was merely $9.8 \times 10^{-8}\,s^{-1}$, which was an order of magnitude lower than that in the rest of daytime. These results underscore the fact that enhanced ALWC during the daytime led to an insufficiently rapid heterogeneous reaction of IEPOX and finally diminished the $BSOA_I$ formation.

To elucidate the key factors that affect BSOA formation aloft, a random forest (RF) analysis was conducted for the daytime samples at the MS site. The RF model commendably highlighted the significance of the factors contributing to $BSOA_I$ formation, as evidenced by the robust correlations between the predicted and observed data for both the training and testing datasets ($R^2 > 0.8$, Table S1 in the Supplement), along with minimal error metrics. As shown in Fig. 5d, the daytime $BSOA_I$ concentration was largely affected by the ozone ($\sim 29\,\%$), with a robust positive correlation between them (Fig. 5a). This indicated that enhanced O_3 is likely to augment isoprene oxidation products aloft. Additionally, NO_2 and ALWC also play pivotal roles in $BSOA_I$ formation, with the importance of $\sim 19\,\%$ and $13\,\%$, respectively. These findings further corroborated the fact that the enhanced NO_x may lead to an impedimental effect on the daytime BSOA formation in the upper boundary layer of Mt. Hua. Such a limiting effect on isoprene-derived SOA formation under a high-NO_x scenario was also found in eastern China and the Amazon (Zhang et al., 2017; De Sa et al., 2017).

4 Summary and conclusion

The $PM_{2.5}$ samples with 4 h intervals were synchronously collected at the mountain foot and mountainside of Mt. Hua to elucidate the chemical evolution and spatiotemporal differences of the organic matter between the two sites. At the MF site, the anthropogenic emissions, such as biomass burning and fossil fuel combustion, were identified as substantial contributors to the OM, accounting for more than $70\,\%$ of total OM, whereas only $\sim 24\,\%$ of OM aloft was derived from anthropogenic emissions, with biogenic secondary organic aerosol ($43\,\%$) emerging as the predominant OM source aloft.

Three distinct types of BSOA tracers were identified, predominantly featuring isoprene-derived species. At the MF site, most of the BSOA tracers were more abundant during the daytime and peaked at 12:00–16:00 LT, indicative of photochemical oxidation as the primary formation pathway, whereas there is a marked decrease in the absolute concentration and relative abundance of daytime isoprene-derived tracers in the upper atmosphere. This decline can be attributed to the intrusion of ground-level NO_x, which significantly modifies $BSOA_I$ formation at higher altitudes by inhibiting the $HO_2\bullet$ oxidative pathway. Additionally, further formation of sulfate in a lifting air mass moderately enhanced ALWC aloft, leading to a low IEPOX reactive uptake on the particle surface, which would also limit the daytime $BSOA_I$ formation aloft. Unfortunately, our limited data do not allow us to peer into the fundamental mechanistic and kinetic details of this process. All these findings highlighted the complex and regional variability of the influences of NO_x on BSOA formation. Over the past decade, the atmospheric environment in China has undergone substantial changes due to unevenly implemented emission controls, resulting in much higher levels of NO_2 compared with SO_2 (Zheng et al., 2018). These alterations in pollutant emissions could substantially affect BSOA formation. Thus, there is an urgent need for long-term characterization of BSOA to better assess its potential impacts on radiative forcing and human health and to fully understand the anthropogenic–biogenic interactions.

Data availability. The data used in this study are freely available at https://doi.org/10.5281/zenodo.15164940 (Wu, 2025). Meteorological data and hourly $PM_{2.5}$, NO_2, and O_3 concentrations can be obtained from https://doi.org/10.5281/zenodo.7413640 (Wu, 2022).

Supplement. The supplement related to this article is available online at https://doi.org/10.5194/acp-25-11975-2025-supplement.

Author contributions. GW designed research and contributed analytic tools. CW, CC, and JL collected the samples. CW and YC conducted the sample analysis. CW and GW performed the data interpretation. CW wrote the paper. All authors contributed to the paper with useful scientific discussions.

Competing interests. The contact author has declared that none of the authors has any competing interests.

Disclaimer. Publisher's note: Copernicus Publications remains neutral with regard to jurisdictional claims made in the text, published maps, institutional affiliations, or any other geographical rep-

resentation in this paper. While Copernicus Publications makes every effort to include appropriate place names, the final responsibility lies with the authors.

Acknowledgements. This work was financially supported by the National Natural Science Foundation of China (grant nos. 42477097, 42130704) and the National Key Research and Development Program of China (grant no. 2023YFC3707401).

Financial support. This research has been supported by the National Natural Science Foundation of China (grant nos. 42477097 and 42130704) and the National Key Research and Development Program of China (grant no. 2023YFC3707401).

Review statement. This paper was edited by Jason Surratt and reviewed by two anonymous referees.

References

Aoki, E., Sarrimanolis, J. N., Lyon, S. A., and Elrod, M. J.: Determining the Relative Reactivity of Sulfate, Bisulfate, and Organosulfates with Epoxides on Secondary Organic Aerosol, ACS Earth and Space Chemistry, 4, 1793–1801, https://doi.org/10.1021/acsearthspacechem.0c00178, 2020.

Armstrong, N. C., Chen, Y., Cui, T., Zhang, Y., Christensen, C., Zhang, Z., Turpin, B. J., Chan, M. N., Gold, A., Ault, A. P., and Surratt, J. D.: Isoprene Epoxydiol-Derived Sulfated and Nonsulfated Oligomers Suppress Particulate Mass Loss during Oxidative Aging of Secondary Organic Aerosol, Environ. Sci. Technol., 56, https://doi.org/10.1021/acs.est.2c03200, 2022.

Bhat, S. and Fraser, M. P.: Primary source attribution and analysis of α-pinene photooxidation products in Duke Forest, North Carolina, Atmos. Environ., 41, 2958–2966, https://doi.org/10.1016/j.atmosenv.2006.12.018, 2007.

Coggon, M. M., Gkatzelis, G. I., McDonald, B. C., Gilman, J. B., Schwantes, R. H., Abuhassan, N., Aikin, K. C., Arend, M. F., Berkoff, T. A., Brown, S. S., Campos, T. L., Dickerson, R. R., Gronoff, G., Hurley, J. F., Isaacman-VanWertz, G., Koss, A. R., Li, M., McKeen, S. A., Moshary, F., Peischl, J., Pospisilova, V., Ren, X., Wilson, A., Wu, Y., Trainer, M., and Warneke, C.: Volatile chemical product emissions enhance ozone and modulate urban chemistry, P. Natl. Acad. Sci. USA, 118, https://doi.org/10.1073/pnas.2026653118, 2021.

Cooke, M. E., Waters, C. M., Asare, J. Y., Mirrielees, J. A., Holen, A. L., Frauenheim, M. P., Zhang, Z., Gold, A., Pratt, K. A., Surratt, J. D., Ladino, L. A., and Ault, A. P.: Atmospheric Aerosol Sulfur Distribution and Speciation in Mexico City: Sulfate, Organosulfates, and Isoprene-Derived Secondary Organic Aerosol from Low NO Pathways, ACS ES&T Air, 1, 1037–1052, https://doi.org/10.1021/acsestair.4c00048, 2024a.

Cooke, M. E., Armstrong, N. C., Fankhauser, A. M., Chen, Y., Lei, Z., Zhang, Y., Ledsky, I. R., Turpin, B. J., Zhang, Z., Gold, A., McNeill, V. F., Surratt, J. D., and Ault, A. P.: Decreases in Epoxide-Driven Secondary Organic Aerosol Production under Highly Acidic Conditions: The Importance of Acid-Base Equilibria, Environ. Sci. Technol., 58, 10675–10684, https://doi.org/10.1021/acs.est.3c10851, 2024b.

de Sá, S. S., Palm, B. B., Campuzano-Jost, P., Day, D. A., Newburn, M. K., Hu, W., Isaacman-VanWertz, G., Yee, L. D., Thalman, R., Brito, J., Carbone, S., Artaxo, P., Goldstein, A. H., Manzi, A. O., Souza, R. A. F., Mei, F., Shilling, J. E., Springston, S. R., Wang, J., Surratt, J. D., Alexander, M. L., Jimenez, J. L., and Martin, S. T.: Influence of urban pollution on the production of organic particulate matter from isoprene epoxydiols in central Amazonia, Atmos. Chem. Phys., 17, 6611–6629, https://doi.org/10.5194/acp-17-6611-2017, 2017.

Dong, X., Liu, Y., Li, X., Yue, M., Liu, Y., Ma, Z., Zheng, H., Huang, R., and Wang, M.: Modeling Analysis of Biogenic Secondary Organic Aerosol Dependence on Anthropogenic Emissions in China, Environ. Sci. Tech. Let., 9, 286–292, https://doi.org/10.1021/acs.estlett.2c00104, 2022.

Drozd, G. T., Woo, J. L., and McNeill, V. F.: Self-limited uptake of α-pinene oxide to acidic aerosol: the effects of liquid–liquid phase separation and implications for the formation of secondary organic aerosol and organosulfates from epoxides, Atmos. Chem. Phys., 13, 8255–8263, https://doi.org/10.5194/acp-13-8255-2013, 2013.

Eddingsaas, N. C., VanderVelde, D. G., and Wennberg, P. O.: Kinetics and Products of the Acid-Catalyzed Ring-Opening of Atmospherically Relevant Butyl Epoxy Alcohols, J. Phys. Chem.-USA, 114, 8106–8113, https://doi.org/10.1021/jp103907c, 2010.

Elser, M., Huang, R.-J., Wolf, R., Slowik, J. G., Wang, Q., Canonaco, F., Li, G., Bozzetti, C., Daellenbach, K. R., Huang, Y., Zhang, R., Li, Z., Cao, J., Baltensperger, U., El-Haddad, I., and Prévôt, A. S. H.: New insights into $PM_{2.5}$ chemical composition and sources in two major cities in China during extreme haze events using aerosol mass spectrometry, Atmos. Chem. Phys., 16, 3207–3225, https://doi.org/10.5194/acp-16-3207-2016, 2016.

Fu, P., Kawamura, K., and Miura, K.: Molecular characterization of marine organic aerosols collected during a round-the-world cruise, J. Geophys. Res.-Atmos., 116, https://doi.org/10.1029/2011jd015604, 2011.

Fu, P., Kawamura, K., Chen, J., and Miyazaki, Y.: Secondary Production of Organic Aerosols from Biogenic VOCs over Mt. Fuji, Japan, Environ. Sci. Technol., 48, 8491–8497, https://doi.org/10.1021/es500794d, 2014.

Fu, P. Q., Kawamura, K., Chen, J., Li, J., Sun, Y. L., Liu, Y., Tachibana, E., Aggarwal, S. G., Okuzawa, K., Tanimoto, H., Kanaya, Y., and Wang, Z. F.: Diurnal variations of organic molecular tracers and stable carbon isotopic composition in atmospheric aerosols over Mt. Tai in the North China Plain: an influence of biomass burning, Atmos. Chem. Phys., 12, 8359–8375, https://doi.org/10.5194/acp-12-8359-2012, 2012.

Gagan, S., Sarang, K., Rudzinski, K. J., Liu, R., Szmigielski, R., and Zhang, Y.: Synthetic strategies for oxidation products from biogenic volatile organic compounds in the atmosphere: A review, Atmos. Environ., 312, https://doi.org/10.1016/j.atmosenv.2023.120017, 2023.

Gaston, C. J., Riedel, T. P., Zhang, Z., Gold, A., Surratt, J. D., and Thornton, J. A.: Reactive Uptake of an Isoprene-Derived Epoxydiol to Submicron Aerosol Particles, Environ. Sci. Technol., 48, 11178–11186, https://doi.org/10.1021/es5034266, 2014.

Guenther, A. B., Jiang, X., Heald, C. L., Sakulyanontvittaya, T., Duhl, T., Emmons, L. K., and Wang, X.: The Model of

Emissions of Gases and Aerosols from Nature version 2.1 (MEGAN2.1): an extended and updated framework for modeling biogenic emissions, Geosci. Model Dev., 5, 1471–1492, https://doi.org/10.5194/gmd-5-1471-2012, 2012.

Hallquist, M., Wenger, J. C., Baltensperger, U., Rudich, Y., Simpson, D., Claeys, M., Dommen, J., Donahue, N. M., George, C., Goldstein, A. H., Hamilton, J. F., Herrmann, H., Hoffmann, T., Iinuma, Y., Jang, M., Jenkin, M. E., Jimenez, J. L., Kiendler-Scharr, A., Maenhaut, W., McFiggans, G., Mentel, Th. F., Monod, A., Prévôt, A. S. H., Seinfeld, J. H., Surratt, J. D., Szmigielski, R., and Wildt, J.: The formation, properties and impact of secondary organic aerosol: current and emerging issues, Atmos. Chem. Phys., 9, 5155–5236, https://doi.org/10.5194/acp-9-5155-2009, 2009.

Hodnebrog, O., Myhre, G., and Samset, B. H.: How shorter black carbon lifetime alters its climate effect, Nat. Commun., 5, https://doi.org/10.1038/ncomms6065, 2014.

Hodzic, A., Kasibhatla, P. S., Jo, D. S., Cappa, C. D., Jimenez, J. L., Madronich, S., and Park, R. J.: Rethinking the global secondary organic aerosol (SOA) budget: stronger production, faster removal, shorter lifetime, Atmos. Chem. Phys., 16, 7917–7941, https://doi.org/10.5194/acp-16-7917-2016, 2016.

Isaacman-VanWertz, G., Yee, L. D., Kreisberg, N. M., Wernis, R., Moss, J. A., Hering, S. V., de Sa, S. S., Martin, S. T., Alexander, M. L., Palm, B. B., Hu, W., Campuzano-Jost, P., Day, D. A., Jimenez, J. L., Riva, M., Surratte, J. D., Viegas, J., Manzi, A., Edgerton, E., Baumann, K., Souza, R., Artaxo, P., and Goldstein, A. H.: Ambient Gas-Particle Partitioning of Tracers for Biogenic Oxidation, Environ. Sci. Technol., 50, 9952–9962, https://doi.org/10.1021/acs.est.6b01674, 2016.

Jaoui, M., Leungsakul, S., and Kamens, R. M.: Gas and particle products distribution from the reaction of β-caryophyllene with ozone, J. Atmos. Chem., 45, 261–287, https://doi.org/10.1023/a:1024263430285, 2003.

Jaoui, M., Kleindienst, T. E., Lewandowski, M., Offenberg, J. H., and Edney, E. O.: Identification and quantification of aerosol polar oxygenated compounds bearing carboxylic or hydroxyl groups. 2. Organic tracer compounds from monoterpenes, Environ. Sci. Technol., 39, 5661–5673, https://doi.org/10.1021/es048111b, 2005.

Jaoui, M., Lewandowski, M., Kleindienst, T. E., Offenberg, J. H., and Edney, E. O.: β-caryophyllinic acid:: An atmospheric tracer for β-caryophyllene secondary organic aerosol, Geophys. Res. Lett., 34, https://doi.org/10.1029/2006gl028827, 2007.

Kelly, J. M., Doherty, R. M., O'Connor, F. M., and Mann, G. W.: The impact of biogenic, anthropogenic, and biomass burning volatile organic compound emissions on regional and seasonal variations in secondary organic aerosol, Atmos. Chem. Phys., 18, 7393–7422, https://doi.org/10.5194/acp-18-7393-2018, 2018.

Kroll, J. H., Ng, N. L., Murphy, S. M., Flagan, R. C., and Seinfeld, J. H.: Secondary organic aerosol formation from isoprene photooxidation, Environ. Sci. Technol., 40, 1869–1877, https://doi.org/10.1021/es0524301, 2006.

Lee, A. K. Y., Abbatt, J. P. D., Leaitch, W. R., Li, S.-M., Sjostedt, S. J., Wentzell, J. J. B., Liggio, J., and Macdonald, A. M.: Substantial secondary organic aerosol formation in a coniferous forest: observations of both day- and nighttime chemistry, Atmos. Chem. Phys., 16, 6721–6733, https://doi.org/10.5194/acp-16-6721-2016, 2016.

Lei, Z., Chen, Y., Zhang, Y., Cooke, M. E., Ledsky, I. R., Armstrong, N. C., Olson, N. E., Zhang, Z., Gold, A., Surratt, J. D., and Ault, A. P.: Initial pH Governs Secondary Organic Aerosol Phase State and Morphology after Uptake of Isoprene Epoxydiols (IEPDX), Environ. Sci. Technol., 56, 10596–10607, https://doi.org/10.1021/acs.est.2c01579, 2022.

Li, J., Li, J., Wang, G., Ho, K. F., Han, J., Dai, W., Wu, C., Cao, C., and Liu, L.: In-vitro oxidative potential and inflammatory response of ambient $PM_{2.5}$ in a rural region of Northwest China: Association with chemical compositions and source contribution, Environ. Res., 205, https://doi.org/10.1016/j.envres.2021.112466, 2022.

Li, J. J., Wang, G. H., Cao, J. J., Wang, X. M., and Zhang, R. J.: Observation of biogenic secondary organic aerosols in the atmosphere of a mountain site in central China: temperature and relative humidity effects, Atmos. Chem. Phys., 13, 11535–11549, https://doi.org/10.5194/acp-13-11535-2013, 2013.

Lin, Y.-H., Zhang, Z., Docherty, K. S., Zhang, H., Budisulistiorini, S. H., Rubitschun, C. L., Shaw, S. L., Knipping, E. M., Edgerton, E. S., Kleindienst, T. E., Gold, A., and Surratt, J. D.: Isoprene Epoxydiols as Precursors to Secondary Organic Aerosol Formation: Acid-Catalyzed Reactive Uptake Studies with Authentic Compounds, Environ. Sci. Technol., 46, 250–258, https://doi.org/10.1021/es202554c, 2012.

Lin, Y.-H., Zhang, H., Pye, H. O. T., Zhang, Z., Marth, W. J., Park, S., Arashiro, M., Cui, T., Budisulistiorini, H., Sexton, K. G., Vizuete, W., Xie, Y., Luecken, D. J., Piletic, I. R., Edney, E. O., Bartolotti, L. J., Gold, A., and Surratt, J. D.: Epoxide as a precursor to secondary organic aerosol formation from isoprene photooxidation in the presence of nitrogen oxides, P. Natl. Acad. Sci. USA, 110, 6718–6723, https://doi.org/10.1073/pnas.1221150110, 2013.

Liu, J., Russell, L. M., Lee, A. K. Y., McKinney, K. A., Surratt, J. D., and Ziemann, P. J.: Observational evidence for pollution-influenced selective uptake contributing to biogenic secondary organic aerosols in the southeastern US, Geophys. Res. Lett., 44, 8056–8064, https://doi.org/10.1002/2017gl074665, 2017.

Liu, J., D'Ambro, E. L., Lee, B. H., Schobesberger, S., Bell, D. M., Zaveri, R. A., Zelenyuk, A., Thornton, J. A., and Shilling, J. E.: Monoterpene Photooxidation in a Continuous-Flow Chamber: SOA Yields and Impacts of Oxidants, NO_x, and VOC Precursors, Environ. Sci. Technol., 56, 12066–12076, https://doi.org/10.1021/acs.est.2c02630, 2022.

Marais, E. A., Jacob, D. J., Jimenez, J. L., Campuzano-Jost, P., Day, D. A., Hu, W., Krechmer, J., Zhu, L., Kim, P. S., Miller, C. C., Fisher, J. A., Travis, K., Yu, K., Hanisco, T. F., Wolfe, G. M., Arkinson, H. L., Pye, H. O. T., Froyd, K. D., Liao, J., and McNeill, V. F.: Aqueous-phase mechanism for secondary organic aerosol formation from isoprene: application to the southeast United States and co-benefit of SO_2 emission controls, Atmos. Chem. Phys., 16, 1603–1618, https://doi.org/10.5194/acp-16-1603-2016, 2016.

McFiggans, G., Mentel, T. F., Wildt, J., Pullinen, I., Kang, S., Kleist, E., Schmitt, S., Springer, M., Tillmann, R., Wu, C., Zhao, D., Hallquist, M., Faxon, C., Le Breton, M., Hallquist, A. M., Simpson, D., Bergstrom, R., Jenkin, M. E., Ehn, M., Thornton, J. A., Alfarra, M. R., Bannan, T. J., Percival, C. J., Priestley, M., Topping, D., and Kiendler-Scharr, A.:

Secondary organic aerosol reduced by mixture of atmospheric vapours, Nature, 565, 587–593, https://doi.org/10.1038/s41586-018-0871-y, 2019.

Mellouki, A., Wallington, T. J., and Chen, J.: Atmospheric Chemistry of Oxygenated Volatile Organic Compounds: Impacts on Air Quality and Climate, Chem. Rev., 115, 3984–4014, https://doi.org/10.1021/cr500549n, 2015.

Nazarenko, L., Rind, D., Tsigaridis, K., Del Genio, A. D., Kelley, M., and Tausnev, N.: Interactive nature of climate change and aerosol forcing, J. Geophys. Res.-Atmos., 122, 3457–3480, https://doi.org/10.1002/2016jd025809, 2017.

Ng, N. L., Brown, S. S., Archibald, A. T., Atlas, E., Cohen, R. C., Crowley, J. N., Day, D. A., Donahue, N. M., Fry, J. L., Fuchs, H., Griffin, R. J., Guzman, M. I., Herrmann, H., Hodzic, A., Iinuma, Y., Jimenez, J. L., Kiendler-Scharr, A., Lee, B. H., Luecken, D. J., Mao, J., McLaren, R., Mutzel, A., Osthoff, H. D., Ouyang, B., Picquet-Varrault, B., Platt, U., Pye, H. O. T., Rudich, Y., Schwantes, R. H., Shiraiwa, M., Stutz, J., Thornton, J. A., Tilgner, A., Williams, B. J., and Zaveri, R. A.: Nitrate radicals and biogenic volatile organic compounds: oxidation, mechanisms, and organic aerosol, Atmos. Chem. Phys., 17, 2103–2162, https://doi.org/10.5194/acp-17-2103-2017, 2017.

Petit, J. E., Favez, O., Albinet, A., and Canonaco, F.: A user-friendly tool for comprehensive evaluation of the geographical origins of atmospheric pollution: Wind and trajectory analyses, Environ. Modell. Softw., 88, 183–187, https://doi.org/10.1016/j.envsoft.2016.11.022, 2017.

Pétron, G., Harley, P., Greenberg, J., and Guenther, A.: Seasonal temperature variations influence isoprene emission, Geophys. Res. Lett., 28, 1707–1710, https://doi.org/10.1029/2000gl011583, 2001.

Pye, H. O. T., Chan, A. W. H., Barkley, M. P., and Seinfeld, J. H.: Global modeling of organic aerosol: the importance of reactive nitrogen (NO_x and NO_3), Atmos. Chem. Phys., 10, 11261–11276, https://doi.org/10.5194/acp-10-11261-2010, 2010.

Ren, Y., Wang, G., Tao, J., Zhang, Z., Wu, C., Wang, J., Li, J., Wei, J., Li, H., and Meng, F.: Seasonal characteristics of biogenic secondary organic aerosols at Mt. Wuyi in Southeastern China: Influence of anthropogenic pollutants, Environ. Pollut., 252, 493–500, https://doi.org/10.1016/j.envpol.2019.05.077, 2019.

Ridley, D. A., Heald, C. L., Ridley, K. J., and Kroll, J. H.: Causes and consequences of decreasing atmospheric organic aerosol in the United States, P. Natl. Acad. Sci. USA, 115, 290–295, https://doi.org/10.1073/pnas.1700387115, 2018.

Riedel, T. P., Lin, Y.-H., Budisulistiorini, H., Gaston, C. J., Thornton, J. A., Zhang, Z., Vizuete, W., Gold, A., and Surrattt, J. D.: Heterogeneous Reactions of Isoprene-Derived Epoxides: Reaction Probabilities and Molar Secondary Organic Aerosol Yield Estimates, Environ. Sci. Tech. Let., 2, 38–42, https://doi.org/10.1021/ez500406f, 2015.

Riva, M., Chen, Y., Zhang, Y., Lei, Z., Olson, N. E., Boyer, H. C., Narayan, S., Yee, L. D., Green, H. S., Cui, T., Zhang, Z., Baumann, K., Fort, M., Edgerton, E., Budisulistiorini, S. H., Rose, C. A., Ribeiro, I. O., Oliveira, R. L., dos Santos, E. O., Machado, C. M. D., Szopa, S., Zhao, Y., Alves, E. G., de Sa, S. S., Hu, W., Knipping, E. M., Shaw, S. L., Duvoisin Junior, S., de Souza, R. A. F., Palm, B. B., Jimenez, J.-L., Glasius, M., Goldstein, A. H., Pye, H. O. T., Gold, A., Turpin, B. J., Vizuete, W., Martin, S. T., Thornton, J. A., Dutcher, C. S., Ault, A. P., and Surratt, J. D.: Increasing Isoprene Epoxydiol-to-Inorganic Sulfate Aerosol Ratio Results in Extensive Conversion of Inorganic Sulfate to Organosulfur Forms: Implications for Aerosol Physicochemical Properties, Environ. Sci. Technol., 53, 8682–8694, https://doi.org/10.1021/acs.est.9b01019, 2019.

Schauer, J. J., Kleeman, M. J., Cass, G. R., and Simoneit, B. R. T.: Measurement of emissions from air pollution sources.: 2.: C_1 through C_{30} organic compounds from medium duty diesel trucks, Environ. Sci. Technol., 33, 1578–1587, https://doi.org/10.1021/es980081n, 1999.

Scott, C. E., Rap, A., Spracklen, D. V., Forster, P. M., Carslaw, K. S., Mann, G. W., Pringle, K. J., Kivekäs, N., Kulmala, M., Lihavainen, H., and Tunved, P.: The direct and indirect radiative effects of biogenic secondary organic aerosol, Atmos. Chem. Phys., 14, 447–470, https://doi.org/10.5194/acp-14-447-2014, 2014.

Shrivastava, M., Cappa, C. D., Fan, J., Goldstein, A. H., Guenther, A. B., Jimenez, J. L., Kuang, C., Laskin, A., Martin, S. T., Ng, N. L., Petaja, T., Pierce, J. R., Rasch, P. J., Roldin, P., Seinfeld, J. H., Shilling, J., Smith, J. N., Thornton, J. A., Volkamer, R., Wang, J., Worsnop, D. R., Zaveri, R. A., Zelenyuk, A., and Zhang, Q.: Recent advances in understanding secondary organic aerosol: Implications for global climate forcing, Rev. Geophys., 55, 509–559, https://doi.org/10.1002/2016rg000540, 2017.

Surratt, J. D., Murphy, S. M., Kroll, J. H., Ng, a. L. N., Hildebrandt, L., Sorooshian, A., Szmigielski, R., Vermeylen, R., Maenhaut, W., Claeys, M., Flagan, R. C., and Seinfeld, J. H.: Chemical composition of secondary organic aerosol formed from the photooxidation of isoprene, J. Phys. Chem.-USA, 110, 9665–9690, https://doi.org/10.1021/jp061734m, 2006.

Surratt, J. D., Chan, A. W. H., Eddingsaas, N. C., Chan, M., Loza, C. L., Kwan, A. J., Hersey, S. P., Flagan, R. C., Wennberg, P. O., and Seinfeld, J. H.: Reactive intermediates revealed in secondary organic aerosol formation from isoprene, P. Natl. Acad. Sci. USA, 107, 6640–6645, https://doi.org/10.1073/pnas.0911114107, 2010.

Szmigielski, R., Surratt, J. D., Vermeylen, R., Szmigielska, K., Kroll, J. H., Ng, N. L., Murphy, S. M., Sorooshian, A., Seinfeld, J. H., and Claeys, M.: Characterization of 2-methylglyceric acid oligomers in secondary organic aerosol formed from the photooxidation of isoprene using trimethylsilylation and gas chromatography/ion trap mass spectrometry, J. Mass Spectrom., 42, 101–116, https://doi.org/10.1002/jms.1146, 2007.

Thornton, J. A., Shilling, J. E., Shrivastava, M., D'Ambro, E. L., Zawadowicz, M. A., and Liu, J.: A Near-Explicit Mechanistic Evaluation of Isoprene Photochemical Secondary Organic Aerosol Formation and Evolution: Simulations of Multiple Chamber Experiments with and without Added NO_x, ACS Earth and Space Chemistry, 4, 1161–1181, https://doi.org/10.1021/acsearthspacechem.0c00118, 2020.

Wan, X., Kang, S., Rupakheti, M., Zhang, Q., Tripathee, L., Guo, J., Chen, P., Rupakheti, D., Panday, A. K., Lawrence, M. G., Kawamura, K., and Cong, Z.: Molecular characterization of organic aerosols in the Kathmandu Valley, Nepal: insights into primary and secondary sources, Atmos. Chem. Phys., 19, 2725–2747, https://doi.org/10.5194/acp-19-2725-2019, 2019.

Wang, G., Zhang, R., Gomez, M. E., Yang, L., Zamora, M. L., Hu, M., Lin, Y., Peng, J., Guo, S., Meng, J., Li, J., Cheng, C.,

Hu, T., Ren, Y., Wang, Y., Gao, J., Cao, J., An, Z., Zhou, W., Li, G., Wang, J., Tian, P., Marrero-Ortiz, W., Secrest, J., Du, Z., Zheng, J., Shang, D., Zeng, L., Shao, M., Wang, W., Huang, Y., Wang, Y., Zhu, Y., Li, Y., Hu, J., Pan, B., Cai, L., Cheng, Y., Ji, Y., Zhang, F., Rosenfeld, D., Liss, P. S., Duce, R. A., Kolb, C. E., and Molina, M. J.: Persistent sulfate formation from London Fog to Chinese haze, P. Natl. Acad. Sci. USA, 113, 13630–13635, https://doi.org/10.1073/pnas.1616540113, 2016.

Wang, G. H. and Kawamura, K.: Molecular characteristics of urban organic aerosols from Nanjing: A case study of a mega-city in China, Environ. Sci. Technol., 39, 7430–7438, https://doi.org/10.1021/es051055+, 2005.

Wang, G. H., Li, J. J., Cheng, C. L., Zhou, B. H., Xie, M. J., Hu, S. Y., Meng, J. J., Sun, T., Ren, Y. Q., Cao, J. J., Liu, S. X., Zhang, T., and Zhao, Z. Z.: Observation of atmospheric aerosols at Mt. Hua and Mt. Tai in central and east China during spring 2009 – Part 2: Impact of dust storm on organic aerosol composition and size distribution, Atmos. Chem. Phys., 12, 4065–4080, https://doi.org/10.5194/acp-12-4065-2012, 2012.

Wang, W., Kourtchev, I., Graham, B., Cafmeyer, J., Maenhaut, W., and Claeys, M.: Characterization of oxygenated derivatives of isoprene related to 2-methyltetrols in Amazonian aerosols using trimethylsilylation and gas chromatography/ion trap mass spectrometry, Rapid Commun. Mass Sp., 19, 1343–1351, https://doi.org/10.1002/rcm.1940, 2005.

Wang, W., Wu, M. H., Li, L., Zhang, T., Liu, X. D., Feng, J. L., Li, H. J., Wang, Y. J., Sheng, G. Y., Claeys, M., and Fu, J. M.: Polar organic tracers in $PM_{2.5}$ aerosols from forests in eastern China, Atmos. Chem. Phys., 8, 7507–7518, https://doi.org/10.5194/acp-8-7507-2008, 2008.

Wang, Y., Meng, J., Huang, T., Ma, J., Wang, Y., Zhang, X., Guo, Q., Yang, J., and Hou, Z.: Contrasting molecular characteristics and formation mechanisms of biogenic and anthropogenic secondary organic aerosols at the summit and foot of Mt. Huang, East China, Sci. Total Environ., 895, https://doi.org/10.1016/j.scitotenv.2023.165116, 2023.

Wu, C.: Synchronous observation of aerosol at Mt. Hua, Version 1, Zenodo [data set], https://doi.org/10.5281/zenodo.7413640, 2022.

Wu, C.: Synchronous observation of biogenic secondary organic aerosol at Mt. Hua, Zenodo [data set], https://doi.org/10.5281/zenodo.15164940, 2025.

Wu, C., Cao, C., Li, J., Lv, S., Li, J., Liu, X., Zhang, S., Liu, S., Zhang, F., Meng, J., and Wang, G.: Different physicochemical behaviors of nitrate and ammonium during transport: a case study on Mt. Hua, China, Atmos. Chem. Phys., 22, 15621–15635, https://doi.org/10.5194/acp-22-15621-2022, 2022.

Wu, C., Liu, X., Zhang, K., Zhang, S., Cao, C., Li, J., Li, R., Zhang, F., and Wang, G.: Measurement report: Formation of tropospheric brown carbon in a lifting air mass, Atmos. Chem. Phys., 24, 9263–9275, https://doi.org/10.5194/acp-24-9263-2024, 2024.

Wu, K., Yang, X., Chen, D., Gu, S., Lu, Y., Jiang, Q., Wang, K., Ou, Y., Qian, Y., Shao, P., and Lu, S.: Estimation of biogenic VOC emissions and their corresponding impact on ozone and secondary organic aerosol formation in China, Atmos. Res., 231, https://doi.org/10.1016/j.atmosres.2019.104656, 2020.

Xu, L., Kollman, M. S., Song, C., Shilling, J. E., and Ng, N. L.: Effects of NO_x on the Volatility of Secondary Organic Aerosol from Isoprene Photooxidation, Environ. Sci. Technol., 48, 2253–2262, https://doi.org/10.1021/es404842g, 2014.

Xu, L., Guo, H., Boyd, C. M., Klein, M., Bougiatioti, A., Cerully, K. M., Hite, J. R., Isaacman-VanWertz, G., Kreisberg, N. M., Knote, C., Olson, K., Koss, A., Goldstein, A. H., Hering, S. V., de Gouw, J., Baumann, K., Lee, S.-H., Nenes, A., Weber, R. J., and Ng, N. L.: Effects of anthropogenic emissions on aerosol formation from isoprene and monoterpenes in the southeastern United States, P. Natl. Acad. Sci. USA, 112, 37–42, https://doi.org/10.1073/pnas.1417609112, 2015.

Xu, L., Middlebrook, A. M., Liao, J., de Gouw, J. A., Guo, H., Weber, R. J., Nenes, A., Lopez-Hilfiker, F. D., Lee, B. H., Thornton, J. A., Brock, C. A., Neuman, J. A., Nowak, J. B., Pollack, I. B., Welti, A., Graus, M., Warneke, C., and Ng, N. L.: Enhanced formation of isoprene-derived organic aerosol in sulfur-rich power plant plumes during Southeast Nexus, J. Geophys. Res.-Atmos., 121, 11137–11153, https://doi.org/10.1002/2016jd025156, 2016.

Xu, X., Wang, G., Gao, Y., Zhang, S., Chen, L., Li, R., Li, Z., and Li, R.: Smog chamber study on the NO_x dependence of SOA from isoprene photo-oxidation: implication on RO2 chemistry, Journal of Environmental Sciences, https://doi.org/10.1016/j.jes.2025.05.024, 2025.

Yan, J., Armstrong, N. C., Kolozsvari, K. R., Waters, C. M., Xiao, Y., Fankhauser, A. M., Cooke, M. E., Frauenheim, M., Buchenau, N. A., Parham, R. L., Zhang, Z., Turpin, B. J., Lambe, A. T., Gold, A., Ault, A. P., and Surratt, J. D.: Effect of Initial Seed Aerosol Acidity on the Kinetics and Products of Heterogeneous Hydroxyl Radical Oxidation of Isoprene Epoxydiol-Derived Secondary Organic Aerosol, J. Phys. Chem.-USA, 129, 4132–4147, https://doi.org/10.1021/acs.jpca.4c08082, 2025.

Ye, J., Batista, C. E., Guimaraes, P. C., Ribeiro, I. O., Vidoudez, C., Barbosa, R. G., Oliveira, R. L., Ma, Y., Jardine, K. J., Surratt, J. D., Guenther, A. B., Souza, R. A. F., and Martin, S. T.: Near-canopy horizontal concentration heterogeneity of semivolatile oxygenated organic compounds and implications for 2-methyltetrols primary emissions, Environmental Science-Atmospheres, 1, 8–20, https://doi.org/10.1039/d0ea00006j, 2021.

Yi, Y., Meng, J., Hou, Z., Wang, G., Zhou, R., Li, Z., Li, Y., Chen, M., Liu, X., Li, H., and Yan, L.: Contrasting compositions and sources of organic aerosol markers in summertime $PM_{2.5}$ from urban and mountainous regions in the North China Plain, Sci. Total Environ., 766, https://doi.org/10.1016/j.scitotenv.2020.144187, 2021.

Zeng, J., Zhang, Y., Mu, Z., Pang, W., Zhang, H., Wu, Z., Song, W., and Wang, X.: Temperature and light dependency of isoprene and monoterpene emissions from tropical and subtropical trees: Field observations in south China, Appl. Geochem., 155, https://doi.org/10.1016/j.apgeochem.2023.105727, 2023.

Zhang, H., Yee, L. D., Lee, B. H., Curtis, M. P., Worton, D. R., Isaacman-VanWertz, G., Offenberg, J. H., Lewandowski, M., Kleindienst, T. E., Beaver, M. R., Holder, A. L., Lonneman, W. A., Docherty, K. S., Jaoui, M., Pye, H. O. T., Hu, W., Day, D. A., Campuzano-Jost, P., Jimenez, J. L., Guo, H., Weber, R. J., de Gouw, J., Koss, A. R., Edgerton, E. S., Brune, W., Mohr, C., Lopez-Hilfiker, F. D., Lutz, A., Kreisberg, N. M., Spielman, S. R., Hering, S. V., Wilson, K. R., Thornton, J. A., and Goldstein, A. H.: Monoterpenes are the

largest source of summertime organic aerosol in the southeastern United States, P. Natl. Acad. Sci. USA, 115, 2038–2043, https://doi.org/10.1073/pnas.1717513115, 2018a.

Zhang, Q., Zheng, Y., Tong, D., Shao, M., Wang, S., Zhang, Y., Xu, X., Wang, J., He, H., Liu, W., Ding, Y., Lei, Y., Li, J., Wang, Z., Zhang, X., Wang, Y., Cheng, J., Liu, Y., Shi, Q., Yan, L., Geng, G., Hong, C., Li, M., Liu, F., Zheng, B., Cao, J., Ding, A., Gao, J., Fu, Q., Huo, J., Liu, B., Liu, Z., Yang, F., He, K., and Hao, J.: Drivers of improved $PM_{2.5}$ air quality in China from 2013 to 2017, P. Natl. Acad. Sci. USA, 116, 24463–24469, https://doi.org/10.1073/pnas.1907956116, 2019a.

Zhang, Y., Tang, L., Sun, Y., Favez, O., Canonaco, F., Albinet, A., Couvidat, F., Liu, D., Jayne, J. T., Wang, Z., Croteau, P. L., Canagaratna, M. R., Zhou, H.-c., Prevot, A. S. H., and Worsnop, D. R.: Limited formation of isoprene epoxydiols-derived secondary organic aerosol under NO_x-rich environments in Eastern China, Geophys. Res. Lett., 44, 2035–2043, https://doi.org/10.1002/2016gl072368, 2017.

Zhang, Y., Chen, Y., Lambe, A. T., Olson, N. E., Lei, Z., Craig, R. L., Zhang, Z., Gold, A., Onasch, T. B., Jayne, J. T., Worsnop, D. R., Gaston, C. J., Thornton, J. A., Vizuete, W., Ault, A. P., and Surratt, J. D.: Effect of the Aerosol-Phase State on Secondary Organic Aerosol Formation from the Reactive Uptake of Isoprene-Derived Epoxydiols (IEPDX), Environ. Sci. Tech. Let., 5, 167–174, https://doi.org/10.1021/acs.estlett.8b00044, 2018b.

Zhang, Y.-Q., Chen, D.-H., Ding, X., Li, J., Zhang, T., Wang, J.-Q., Cheng, Q., Jiang, H., Song, W., Ou, Y.-B., Ye, P.-L., Zhang, G., and Wang, X.-M.: Impact of anthropogenic emissions on biogenic secondary organic aerosol: observation in the Pearl River Delta, southern China, Atmos. Chem. Phys., 19, 14403–14415, https://doi.org/10.5194/acp-19-14403-2019, 2019b.

Zheng, B., Tong, D., Li, M., Liu, F., Hong, C., Geng, G., Li, H., Li, X., Peng, L., Qi, J., Yan, L., Zhang, Y., Zhao, H., Zheng, Y., He, K., and Zhang, Q.: Trends in China's anthropogenic emissions since 2010 as the consequence of clean air actions, Atmos. Chem. Phys., 18, 14095–14111, https://doi.org/10.5194/acp-18-14095-2018, 2018.

Zheng, Y., Horowitz, L. W., Menzel, R., Paynter, D. J., Naik, V., Li, J., and Mao, J.: Anthropogenic amplification of biogenic secondary organic aerosol production, Atmos. Chem. Phys., 23, 8993–9007, https://doi.org/10.5194/acp-23-8993-2023, 2023.

Zhu, C., Kawamura, K., Fukuda, Y., Mochida, M., and Iwamoto, Y.: Fungal spores overwhelm biogenic organic aerosols in a midlatitudinal forest, Atmos. Chem. Phys., 16, 7497–7506, https://doi.org/10.5194/acp-16-7497-2016, 2016.